17th Brazilian Congress of Thermal Sciences and Engineering
November 25th-28th, 2018, Águas de Lindóia, SP, Brazil

ENCIT-2018-0026
EVALUATING RANS TURBULENCE MODELS TO PREDICT THE AIRFLOW IN A DUCT BEND

Marcos Batistella Lopes
Viviana Cocco Marinani,
Pontifical Catholic University of Paraná, PPGEM, R. Imaculada Conceição, 1155, Curitiba, 80215-901, Brazil
marcos.batistella@pucpr.edu.br
viviana.mariani@pucpr.br

Kátia Cordeiro Mendonça
Engineering School of CESI, LINEACT, Av. Michel Crépeau, Lagord, 17042, France
kcordeiro@cesi.fr

Claudine Béghein
Univesity of La Rochelle, LaSIE, , 23 Av. Albert Einstein, La Rochelle, 17000, France
claudine.beghein@univ-lr.fr

Abstract. *The main objective of this study is to evaluate the accuracy of some Reynolds Averaged Navier-Stokes (RANS) models to predict the behavior of the turbulent flows in a horizontal circular duct bend. The selection of the RANS models tested follows the capability of each model to describe the flow near the wall. Therefore, five turbulence models were selected: three Eddy Viscosity Models (two linear, k-ω SST and LRN (Low Reynolds Number) k-ε of Launder and Sharma, and one non-linear, cubic k-ε of Lien) and two Reynolds Stress Models (Launder Reece Rodi (LRR) and Speziale Sarkar Gatzki (SSG)). The numerical solutions were carried out using Computational Fluid Dynamics (CFD) code OpenFOAM® applied in an incompressible turbulent viscous flow. The grid discretization of the viscous sublayer leads to a refinement near to the walls and a smooth grid expansion ratio from the wall to the core of the pipe. The air flows with a Reynolds number of 6×10^4 through a straight circular duct of 0.104 m diameter followed by a 90° bend with curvature ratio of 4. The principal results were compared in terms of streamwise mean velocity profile and turbulence intensity contours. The turbulence models that performed better according to the velocity fields and turbulence intensity was the SSG. Nevertheless, none of them were able to accurately predict the flow next to the inner wall at the bend outlet.*

Keywords: *duct bend, CFD, turbulence, RANS models.*

1. INTRODUCTION

Heat, ventilation and air conditioning (HVAC) distribution systems are composed of straight ducts and fittings such as elbows (Kuehn *et al.*, 1998). The flow field in curved ducts is more complex than in the straight parts because secondary flows occurs and the flow can be detached from the wall.

A major difficulty for predicting the turbulent flow along a duct bend is due to the change in the direction of the principal flow caused by the wall curvature. The centrifugal forces result in an adverse pressure gradient in the radial direction. This leads to a rise in a secondary motion in which the fluid in the center of the duct is swept towards the outer bend wall and the fluid near the wall returns towards the inner bend wall. These counter-rotating vortices are known as Dean vortices (Dean, 1928).

Another important aspect of the turbulent curved pipe flow is the detachment of the boundary layer in the inner bend wall near the bend outlet and the reattachment in the downstream pipe (Takamura *et al.*, 2012), known as separation region. In addition, boundary layer instabilities can appear in the outer bend wall, the Görtler vortices (Saric, 1994), being counter-rotating vortices aligned in the streamwise direction.

The secondary flows and their impact on the primary flow can be predicted in details by CFD tools (Ferziger and Peric, 2002), helping to the HVAC systems design. Despite this, these tools are being largely used to describe the flow in different engineering applications. However, selecting an appropriate turbulence model is still a delicate task when modeling turbulent flows.

The literature presents several works to evaluate the accuracy of turbulent models in curved pipes. Dutta *et al.* (2016) carried out numerical experiments with the standard *k-ε* turbulence model for several Reynolds numbers in a 90° curved pipe to identify the separation region, they suggested that that turbulence model is valid for a wide range of Reynolds numbers. Kim *et al.* (2014) conducted numerical computations with eleven Eddy Viscosity Models (EVM) characterizing the secondary flow in the downstream pipe of a pipe bend, they indicated that the RNG *k-ε* turbulence model was more

accurate among another RANS models. Tanaka *et al.* (2009) showed that the Large Eddy Simulation (LES) was accurate to predict the characteristics of the flow behavior causing the pressure fluctuation on the wall.

In this study, the turbulent airflow in a 90° bend was modeled, and the numerical results were compared with the experimental results obtained by Sudo *et al.* (1998). The turbulence models were selected according to the computational resources and their capacity of describing the flow near to the walls. The main objective of this study is, therefore, to show the strengths and drawbacks of these models to provide the turbulent flow in several regions of the bend.

2. MODEL DESCRIPTION

Sudo *et al.* (1998) experimentally studied the turbulent airflow in a horizontal circular-section 90° duct bend with smooth walls as illustrated schematically in Fig. 1. The length of the studied upstream region is $N_uD = 100D$, and the length of the studied downstream region is $N_dD = 40D$. The duct diameter (D) is 0.104 m and the curvature ratio is 4, consequently the bend radius (R_b) is 0.208 m.

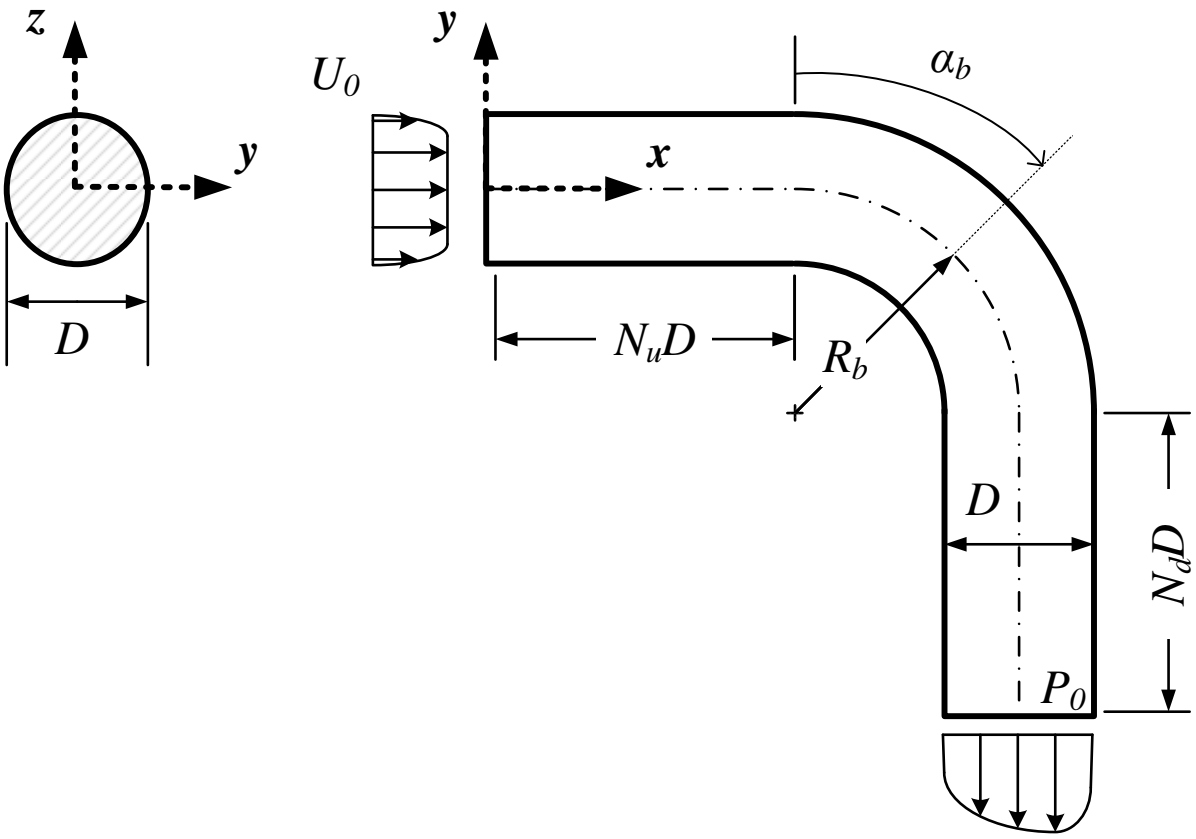

Figure 1. Schematic representation of the experimental apparatus of Sudo *et al.* (1998).

For modeling purpose, a turbulent velocity profile (U_0) was assumed at the inlet of the domain based on the Reynolds number of 6×10^4 given by the average inlet velocity of the experiment and the air properties at 20 °C and 1 atm. Therefore, the straight pipe length was reduced to $N_uD = 10D$ and $N_dD = 20D$ for the upstream and downstream pipes, respectively. A uniform pressure (P_0) of 1 atm was specified in the outlet of the domain and the walls have no-slip boundary conditions for the velocities with special wall functions. Zero gradient boundary condition was set to the pressure at the domain inlet and the walls, and to the velocity and the turbulence parameters at the domain outlet.

2.1 Mathematical model

The Reynolds Averaged Navier-Stokes (RANS) equations are obtained by averaging the transport equations. The mass conservation and momentum equations of a Newtonian and incompressible flow are (Ferziger and Peric, 2002), respectively:

$$\vec{\nabla} \cdot \vec{U} = 0 \tag{1}$$

$$\frac{\partial U_i}{\partial t} + \vec{\nabla} \cdot \left(U_i \vec{U}\right) = -\frac{1}{\rho}\vec{\nabla} \cdot (p\vec{\imath}_i) + \vec{\nabla} \cdot \left(\nu \nabla U_i - \overline{U_\imath U_j}\right) + \frac{F_i}{\rho} \tag{2}$$

where $\vec{U}$ is the fluid averaged velocity vector (ms^{-1}), t is the time (s), ρ is the fluid density (kgm^{-3}), p is the averaged static pressure (Pa), ν is the kinematic fluid viscosity (m^{2}s^{-1}), F_i are the body forces components (N), U_i is the fluid velocity component (ms^{-1}) and $\vec{\imath}_i$ is the Cartesian unit vector (the subscript i indicates the direction of the coordinate x_i).

The RANS turbulence models can be classified as linear Eddy Viscosity Models (EVM), non-linear EVM and Reynolds Stress Models (RSM). In the EVM, the Reynolds tensor $\overline{U_\imath U_j}$, see Eq. (2), is modelled assuming proportionality with the strain rate tensor. The relationship between the stress tensor and the mean flow can be linear or non-linear as indicated by Eqs. (3) and (4), respectively:

$$-\overline{U_\imath U_j} = \nu_t S_{ij} - \frac{2}{3} k \delta_{ij} \tag{3}$$

$$-\overline{U_\imath U_j} = \nu_t S_{ij} - f\left(S_{ij}, \Omega_{ij}\right) - \frac{2}{3} k \delta_{ij} \tag{4}$$

where ν_t is the turbulent kinematic viscosity (m^{2}s^{-1}), δ_{ij} is the Kronecker delta and $f\left(S_{ij}, \Omega_{ij}\right)$ is a non-linear relationship involving the mean strain rate, S_{ij}, and the mean vorticity, Ω_{ij}, given by:

$$S_{ij} = \frac{\partial U_i}{\partial x_j} + \frac{\partial U_j}{\partial x_i} \tag{5}$$

$$\Omega_{ij} = \frac{\partial U_i}{\partial x_j} - \frac{\partial U_j}{\partial x_i} \tag{6}$$

In the RSM, the individual components of the Reynolds tensor are directly computed, consequently seven additional transport equations must be solved: one for the turbulence length scale and six for each component of $\overline{U_\imath U_j}$. The stress transport equations can be written in the following form:

$$\frac{D\overline{U_\imath U_j}}{Dt} = P_{ij} + \phi_{ij} - \varepsilon_{ij} + d_{ij} \tag{7}$$

where P_{ij} is the generation rate of the turbulent stress by the mean strain, d_{ij} is the diffusion rate of the turbulent stress by turbulent and viscous action, ϕ_{ij} and ε_{ij} are processes which are modeled in terms of other turbulent variables such as the Reynolds stress and mean strain.

Table 1 presents the RANS models that were investigated in this study.

Table 1. RANS models investigated.

RANS model	Type	Reference
LRN *k-ε* Launder and Sharma	Linear EVM	Launder and Sharma (1974)
k-ω SST	Linear EVM	Menter (1992)
Lien cubic *k-ε*	Non-linear EVM	Lien *et al.* (1996)
LRR	RSM	Launder *et al.* (1975)
SSG	RSM	Speziale *et al.* (1991)

2.2 Numerical procedure

The toolbox OpenFOAM® was selected to achieve the numerical solution of the governing equations with a transient solver for incompressible turbulent flow based on the PISO algorithm for solving the pressure field (*pisoFoam*). The time step was defined according to the Courant number and the convergence criteria were given as a small variation of the total kinetic energy of the domain.

The meshes were generated with *blockMesh* and the grid sensitive study followed the Grid Convergence Index (GCI) of Roache (1994) with three meshes of 2×10^5, 9×10^5 and 2×10^6 nodes. Figure 2 presents a representation of one of these meshes where the diameter of the duct (D), the size of the viscous sublayer (δ_{vs}) and the distance of the wall to the first node (z_n) are indicated. All meshes were generated with at least 10 nodes in the viscous sublayer and $y^+ \leq 1$. The grid with

9×10^5 cells was selected for further analysis because there was no significant variation regarding the velocity field of the finest grid (not shown here).

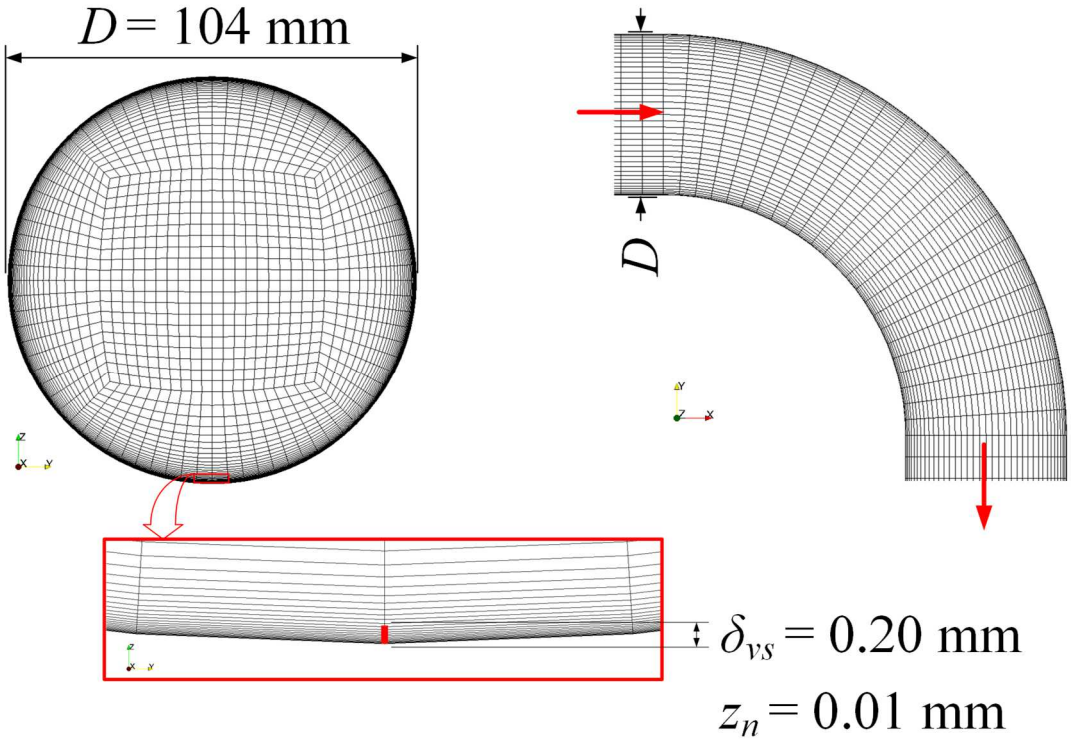

Figure 2. Computational grid with 9×10^5 nodes.

3. RESULTS AND DISCUSSION

The mean velocity in the principal flow direction of the flow on the horizontal plane $z = 0$ is presented in Fig. 3 to Fig. 6. The streamwise mean velocity was dimensionless with the average mean velocity at inlet (U_0) and the dimensionless radial coordinate (r^*) goes from the inner bend wall ($r^* = 0$) to the outer bend wall ($r^* = 1$).

All turbulence models predicted accurately the streamwise velocity from the bend inlet (Fig. 3) to $\alpha_b = 30°$ (Fig. 4). However, the high distortion of the streamwise velocity profile that appears from angles after $\alpha_b = 60°$ (Fig. 5) to the bend outlet (Fig. 6) is not well predicted near the inner bend wall. The linear EVM fail due to the presence of curved streamlines and the secondary motion in the duct bend (Wilcox, 2006). In addition, the distortion could be to high to be predicted by the non-linear EVM and the RSM.

An appropriate statistic method to analyze the deviation of the predicted numerical data of this study from the experimental data of Sudo *et al.* (1998) is the Root Mean Square Error (RMSE), defined as:

$$RMSE = \sqrt{\frac{1}{n}\sum_{i=1}^{n}\left(\varphi_{exp,i} - \varphi_{num,i}\right)^2} \tag{8}$$

where $\varphi_{exp,i}$ is the dimensionless experimental mean velocity, $\varphi_{num,i}$ is the predicted dimensionless mean velocity and n is the number of experimental points.

Figure 7 shows the RMSE regarding each turbulence model tested in this study for the bend angles of 0°, 30°, 60° and 90°. The RMSE is up to 11% at the bend inlet, up to 24% at the bend outlet and has a similar behavior for the turbulence models, i.e., the RMSE increases towards the bend outlet. Among the turbulence models of this study, the RSM SSG achieved a lower RMSE, consequently, this model was the most accurate regarding the mean velocity.

All turbulence models were able to reproduce qualitatively and quantitatively quite well the streamwise dimensionless turbulence intensity in the bend inlet (Fig. 8). In the bend outlet, both linear and non-linear EVM show qualitatively similarity with experimental data, however these models produced weaker values as illustrated in Fig. 9a to 9c. The RSM yielded the best results of dimensionless turbulence intensity in the principal direction of the flow, as presented in Fig. 9d and 9e.

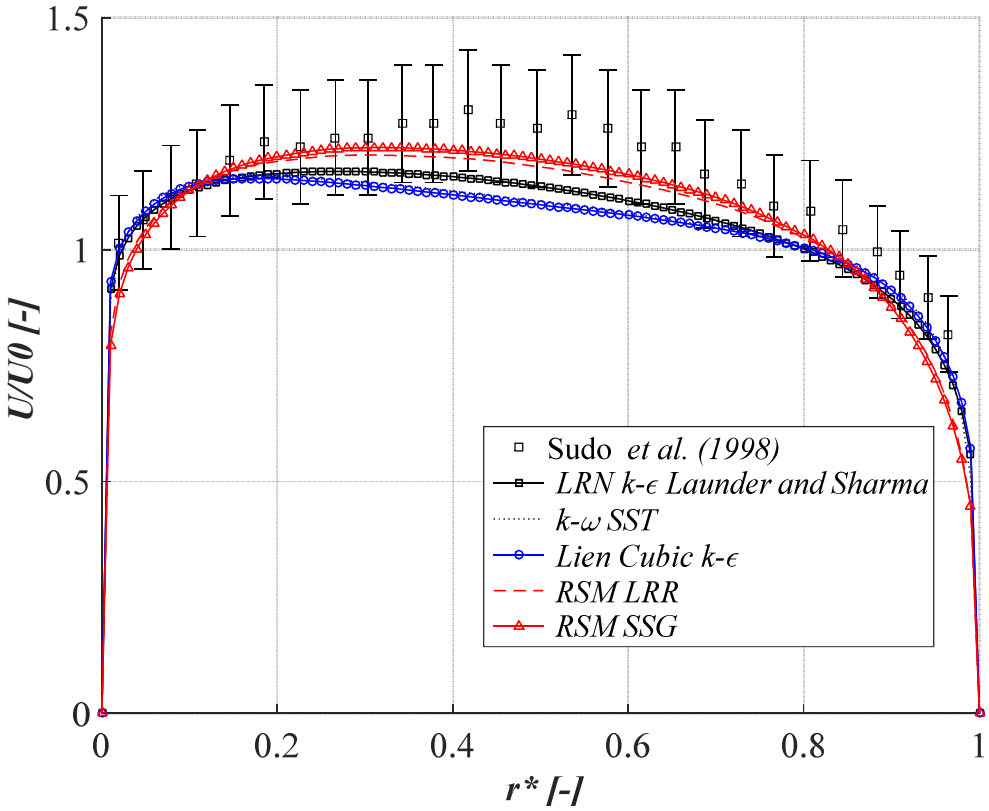

Figure 3. Streamwise dimensionless velocity profile along the duct bend at α_b = 0° (bend inlet).

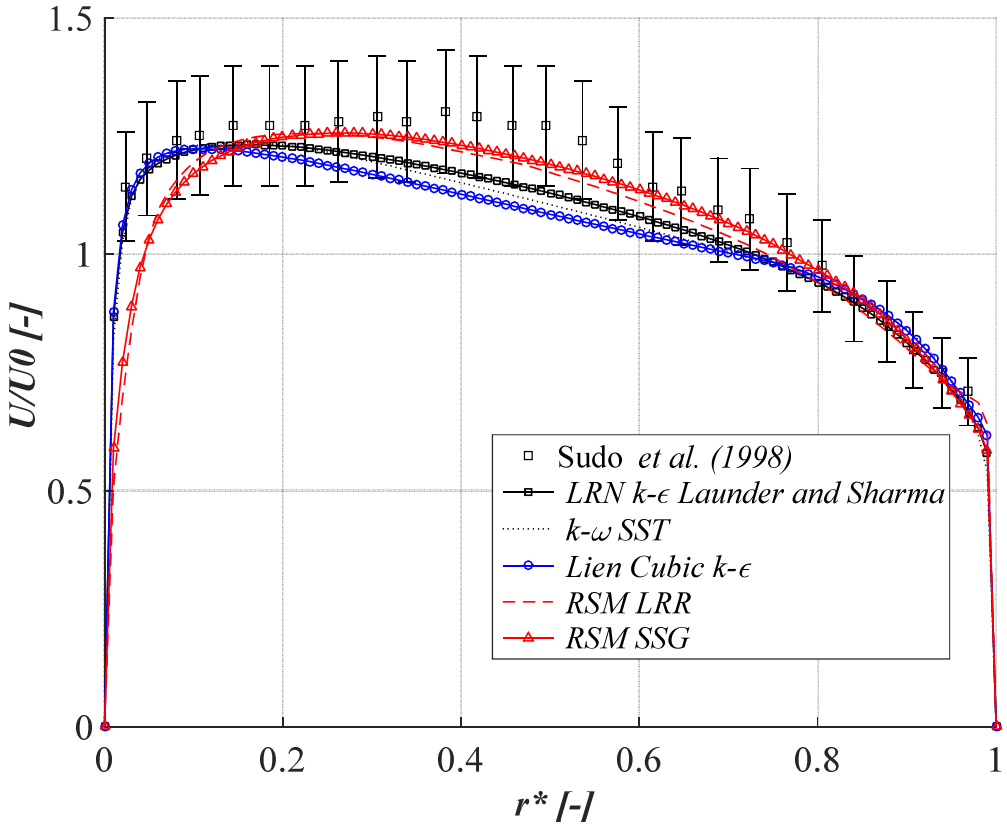

Figure 4. Streamwise dimensionless velocity profile along the duct bend at α_b = 30°.

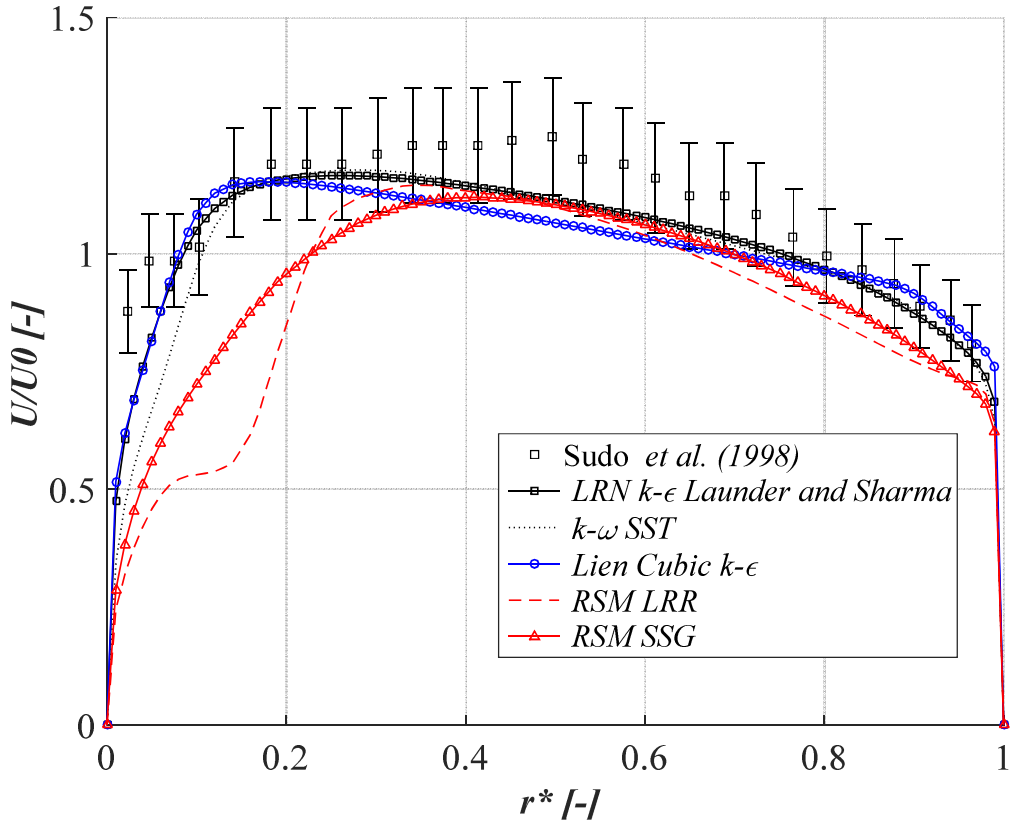

Figure 5. Streamwise dimensionless velocity profile along the duct bend at $\alpha_b = 60°$.

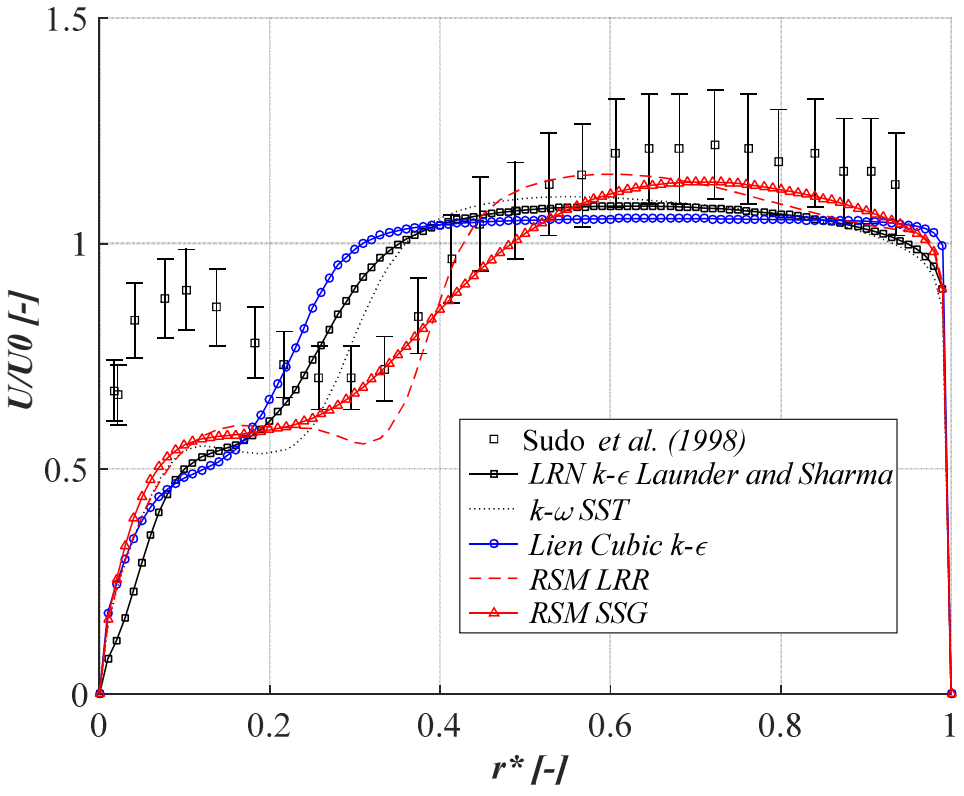

Figure 6. Streamwise dimensionless velocity profile along the duct bend at $\alpha_b = 90°$ (bend outlet).

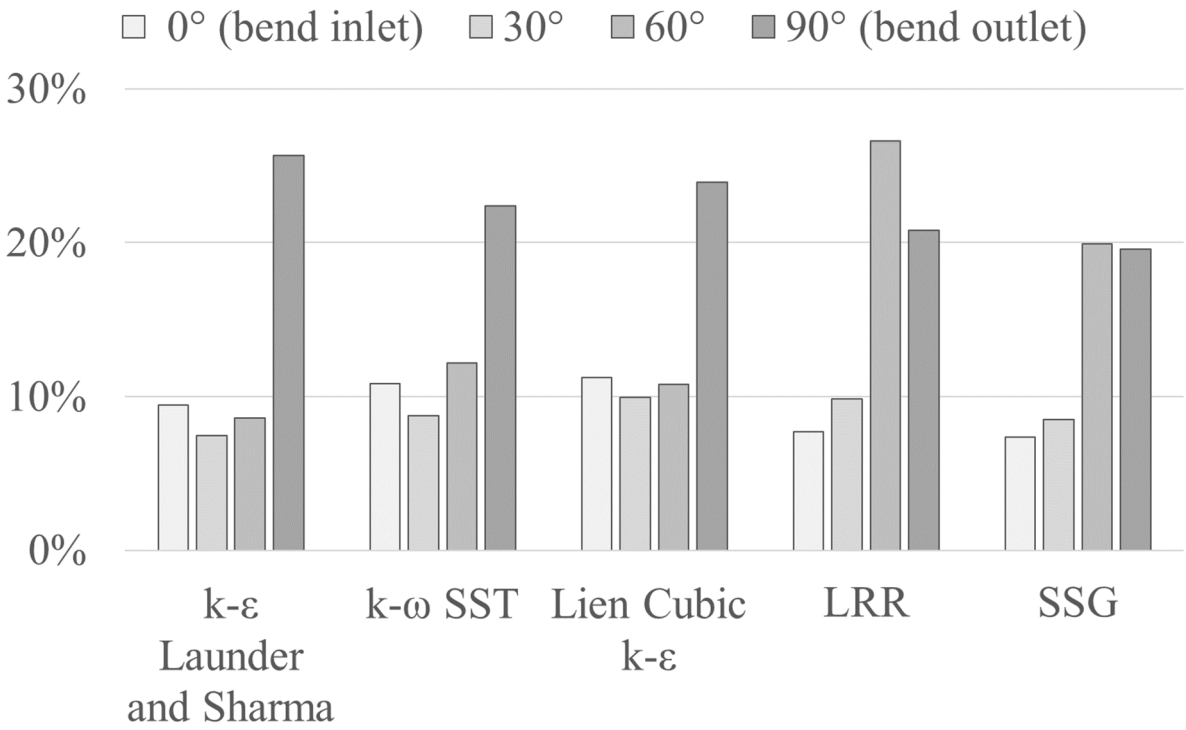

Figure 7. RMSE of dimensionless streamwise velocity for each turbulence model and bend angle.

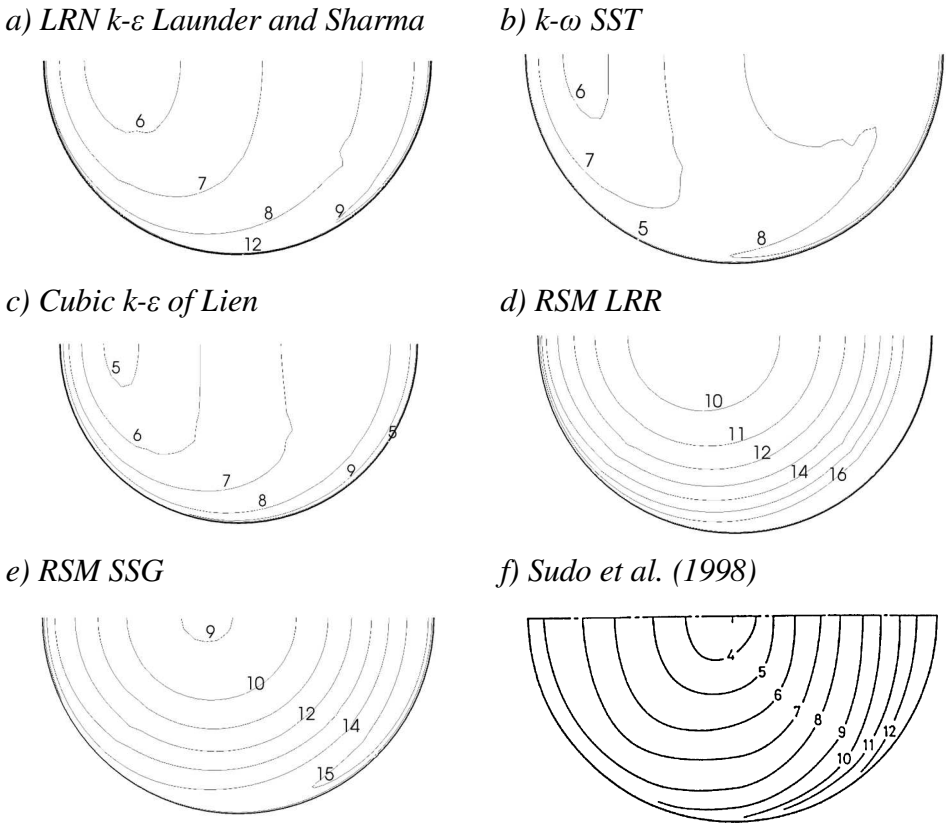

Figure 8. Contours of dimensionless turbulence intensity at streamwise direction at the bend inlet, $\alpha_b = 0°$ (contours of $\sqrt{\overline{u'^2}}/U0 \times 10^2$).

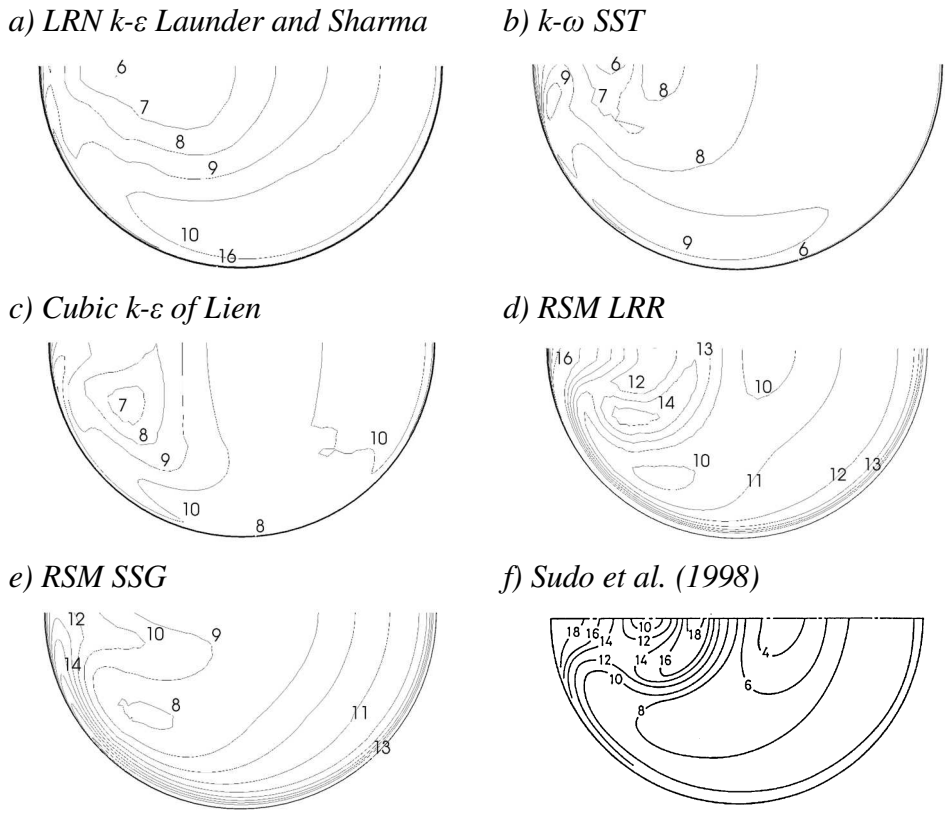

Figure 9. Contours of dimensionless turbulence intensity at streamwise direction at the bend outlet, α_b = 90° (contours of $\sqrt{\overline{v'^2}}/U0 \times 10^2$).

4. CONCLUSIONS

This study focused on the numerical prediction of a turbulent flow in a circular 90° duct with a Reynolds number of 6×10^4, based on the inlet average velocity and duct diameter. The turbulent flow was modelled with linear EVM (*k*-ω SST and LRN *k*-ε Launder and Sharma), non-linear EVM (cubic LRN *k*-ε of Lien *et al.* (1996)) and RSM (LRR and SSG). All turbulence models yielded good results regarding the streamwise velocity in the bend angles of 0° and 30°, however due to the distortion of the velocity profiles the models fail to accurately predict the streamwise velocity near the inner bend wall for bend angles of 60° and 90°. Regarding the velocity fluctuations in the streamwise direction, only the RSM give satisfactory results in the bend outlet. Therefore, among the RANS models tested the RSM seem to better describe this turbulent flow. Future study must consider Large Eddy Simulation (LES) to solve the large eddies of the turbulent flow in the duct bend and, therefore, accurately predict the streamwise velocity in the bend outlet near the inner bend wall.

5. ACKNOWLEDGEMENTS

The authors would like to acknowledge *Fundação Araucária* and the Coordination for the Improvement of Higher Education Personnel (CAPES) for the scholarship provided to the first author, and National Council of Scientific and Technologic Development of Brazil (CNPq) under Grant 303906/2015-4/PQ 1B for the financial support to this study.

6. REFERENCES

Dean, W. R., 1928. "LXXII. The stream-line motion of fluid in a curved pipe (Second paper)". In *The London, Edinburgh, and Dublin Philosophical Magazine and Journal of Science*, v. 5, n. 30.

Dutta, P.; Saha, S. K.; Nandi, N.; Pal, N., 2016. "Numerical study on flow separation in 90° pipe bend under high Reynolds number by k-ε modelling". In *Engineering Science and Technology, an International Journal*, v. 19, n. 2, p. 904–910.

Ferziger, J. H.; Peric, M., 2002. *Computational Methods for Fluid Dynamics*. Springer-Verlag Berlin Heidelberg, 3rd ed..

Kim, J.; Yadav, M.; Kim, S., 2014. "Characteristics of secondary flow induced by 90-degree elbow in turbulent pipe flow". In *Engineering Applications of Computational Fluid Mechanics*, v. 8, n. 2, p. 229–239.

Klebanoff, P. S., 1954. "Characteristics of turbulence in a boundary layer with zero pressure gradient". In *TN 3178*, NACA.

Kuehn, T. H.; Ramsey, J. W.; Threlkeld, J. L., 1998. *Thermal Environmental Engineering*. Prentice Hall, New Jersey, 3rd ed..

Launder, B. E.; Reece, G. J.; Rodi, W., 1975. "Progress in the development of a Reynolds-stress turbulence closure". In *Journal of Fluid Mechanics*, v. 68, n. 3, p. 537.

Launder, B. E.; Sharma, B. I., 1974. "Application of the energy-dissipation model of turbulence to the calculation of flow near a spinning disc". In *Letters in Heat and Mass Transfer*, v. 1, n. 2, p. 131–137.

Lien, F. S.; Chen, W. L.; Leschziner, M. A., 1996. "Low-reynolds-number eddy-viscosity modelling based on non-linear stress-strain/vorticity relations". In *Engineering Turbulence Modelling and Experiments*. p.91–100.

Lin, C. S.; Moulton, R. W.; Putnam, G. L., 1953. "Mass transfer between solid wall and fluid streams: mechanism and eddy distribution relationships in turbulent flow". In *Industrial & Engineering Chemistry*, v. 45, n. 3, p. 636–640.

Menter, F. R., 1992. "Separated adverse pressure gradient flows". In *AIAA Journal*, v. 30, n. 8, p. 2066–2072.

Roache, P. J., 1994. "Perspective: a method for uniform reporting of grid refinement studies". In *Journal of Fluids Engineering*, v. 116, n. 3, p. 405–413.

Saric, W. S., 1994. "Görtler vortices". In *Annual Review of Fluid Mechanics*, v. 26, n. 1, p. 379–409.

Speziale, C. G.; Sarkar, S.; Gatski, T. B., 1991. "Modelling the pressure–strain correlation of turbulence: an invariant dynamical systems approach". In *Journal of Fluid Mechanics*, v. 227, n. 1, p. 245.

Sudo, K.; Sumida, M.; Hibara, H., 1998. "Experimental investigation on turbulent flow in a circular-sectioned 90-degree bend". In *Experiments in Fluids*, v. 25, n. 1, p. 42–49.

Takamura, H.; Ebara, S.; Hashizume, H.; Aizawa, K.; Yamano, H., 2012. "Flow visualization and frequency characteristics of velocity fluctuations of complex turbulent flow in a short elbow piping under high reynolds number condition". In *Journal of Fluids Engineering*, v. 134, n. 10, p. 101201-1 - 101201-8.

Tanaka, M.; Ohshima, H.; Monji, H., 2009. "Numerical investigation of flow structure in pipe elbow with large eddy simulation approach". In *ASME 2009 - PVP2009-77598*, p. 1–10.

Wilcox, D. C., 2006. *Turbulence Modeling for CFD*. DCW Industries.

7. RESPONSIBILITY NOTICE

The authors are the only responsible for the printed material included in this paper.